Kronberg, Rasmus; Hakala, Mikko; Holmberg, Nico; Laasonen, Kari

Hydrogen adsorption on MoS2-surfaces: a DFT study on preferential sites and the effect of sulfur and hydrogen coverage

Published in:
Physical Chemistry Chemical Physics

DOI:
10.1039/c7cp03068a

Published: 07/06/2017

Document Version
Peer reviewed version

Please cite the original version:
Kronberg, R., Hakala, M., Holmberg, N., & Laasonen, K. (2017). Hydrogen adsorption on MoS_2-surfaces: a DFT study on preferential sites and the effect of sulfur and hydrogen coverage. *Physical Chemistry Chemical Physics*, *19*(24), 16231-16241. https://doi.org/10.1039/c7cp03068a

Journal Name

ARTICLE TYPE

Cite this: DOI: 10.1039/xxxxxxxxxx

Hydrogen adsorption on MoS_2-surfaces: A DFT study on preferential sites and the effect of sulfur and hydrogen coverage†

Rasmus Kronberg,[a] Mikko Hakala,[a] Nico Holmberg,[a] and Kari Laasonen*[a]

Received Date
Accepted Date

DOI: 10.1039/xxxxxxxxxx

www.rsc.org/journalname

We report a comprehensive computational study of the intricate structure-property relationships governing the hydrogen adsorption trends on MoS_2 edges with varying S- and H-coverages, as well as provide insights into the role of individual adsorption sites. Additionally, the effect of single- and dual S-vacancies in the basal plane on the adsorption energetics is assessed, likewise with an emphasis on the H-coverage dependency. The employed edge/site-selective approach reveals significant variations in the adsorption free energies, ranging between $\sim \pm 1.0\,\mathrm{eV}$ for the different edges-types and S-saturations, including differences of even as much as $\sim 1.2\,\mathrm{eV}$ between sites on the same edge. The incrementally increasing hydrogen coverage is seen to mainly weaken the adsorption, but intriguingly for certain configurations a stabilizing effect is also observed. The strengthened binding is seen to be coupled with significant surface restructuring, most notably the splitting of terminal S_2-dimers. Our work links the energetics of hydrogen adsorption on 2H-MoS_2 to both static and dynamic geometrical features and quantifies the observed trends as a function of H-coverage, thus illustrating the complex structure/activity relationships of the MoS_2 catalyst. The results of this systematical study aims to serve as guidance for experimentalists by suggesting feasible edge/S-coverage combinations, the synthesis of which would potentially yield the most optimally performing HER-catalysts.

1 Introduction

A sustainable hydrogen economy demands a clean and renewable method for the production of hydrogen gas (H_2). Electrolytic water-splitting, $H_2O\,(l) \rightleftharpoons H_2\,(g) + \frac{1}{2}\,O_2\,(g)$, has been presented as an attractive candidate fulfilling these requirements[1]. When coupled with sustainable energy production, such as solar and wind power, hydrogen could be produced with minimal emissions and in addition function as an energy storage material, smoothing out the intermittency of the renewable resources[2,3]. However, the need of precious platinum group metals (PGM) for the efficient catalysis of the electrochemical half-reactions poses challenges for the large-scale implementation of the electrolytic H_2-production[4]. For now, platinum remains the superior electrocatalyst for the hydrogen evolution reaction (HER, $2H^+\,(aq) + 2e^- \rightleftharpoons H_2\,(g)$), i.e. the cathodic half-reaction of water-splitting, although extensive research to develop cheaper, yet as effective, alternatives from earth-abundant elements has yielded some very promising results[5].

In particular, the group of molybdenum disulfide-based HER-electrocatalysts have presented themselves as interesting and competitive low-cost alternatives to Pt[6–8]. Widespread attempts to optimize and understand the electrocatalytic properties of the material have been initiated by virtue of the early work of Hinnemann *et al.*[6], which initially by both computational and experimental methods demonstrated the potential of MoS_2 as an HER catalyst. The activity of the thermodynamically most stable 2H-MoS_2 polytype with trigonal prismatic D_{3h} coordination[9] has thus been identified to stem from sites located at the sulfur-terminated $(10\bar{1}0)$ Mo- and $(\bar{1}010)$ S-edges, while the preferentially exposed (0001) basal plane has been deemed as catalytically inert[6,10–13]. As such, recent studies have concentrated on the optimization of the material to yield nanostructured configurations with high edge-to-bulk ratios[14–16], as well as preferential tuning of the electronic structure by transition metal doping (PGMs, Co, Ni) and defect-engineering to yield more active sites and also improve the catalytic characteristics of the basal plane[17–21]. Further, maximization of the electron transfer kinetics has been attempted by improving the conductivity of the catalyst through utilization of

[a] Research Group of Computational Chemistry, Department of Chemistry and Materials Science, Aalto University, P.O. Box 16100, FI-00076 Aalto, Finland
* E-mail: kari.laasonen@aalto.fi

† Electronic Supplementary Information (ESI) available: See DOI: 10.1039/b000000x/

metallic phases[22] (1T-MoS_2, octahedral O_h coordination[23]) and conductive support materials, such as graphene and carbon nanotubes[17,24].

Computational studies using density functional theory (DFT) are widely utilized as a complementary method in the experimental search of new potential HER-electrocatalysts[6,13,25–33]. DFT provides means by which to model the electrocatalytically relevant systems at an atomic level and gain detailed insight into the trends and mechanism behind the activity of materials. Generally, a descriptor based approach using the Gibbs free energy of adsorption (ΔG_H) is employed when an efficient evaluation of the catalytic activity is desired[34]. According to the Sabatier principle of heterogeneous catalysis, one of the criteria for optimal activity is a thermoneutral ΔG_H-value, i.e. $\Delta G_H \approx 0\,eV$, as very negative values indicate too strong adsorption which hinders the desorption of products and poisons the catalyst. Conversely, high positive values is a sign of too weak adsorption and thus limited activation and electron transfer kinetics[35]. As a reference, reported ΔG_H-values for Pt and MoS_2 basal plane are on the order of $-0.1\,eV$[25,36] and $1.9\,eV$[18,28], respectively.

In the present article, we report a systematical study of the hydrogen adsorption characteristics of multilayer 2H-MoS_2 edges (Mo-edge, S-edge) as well as of pristine and sulfur deficient, i.e. vacancy containing, basal planes. The main emphasis is on trends observed as a function of varying hydrogen- and sulfur-coverages (θ_H, θ_S). The Mo- and S-edges with varying sulfur-coverages have a considerable amount of structural degrees of freedom for hydrogen adsorption sites, especially if one aims at a systematic study of adsorption energetics as a function of hydrogen coverage. As searching through this geometrical space without any additional constraints would be computationally too demanding, we perform our calculations by coarse-graining the geometrical search space by using for hydrogen a set of plausible local adsorption sites (such as on-top, bridge, hollow, see Section 2.2). This way, the geometrical degrees of freedom can be effectively studied and systematic results are obtained as a function of hydrogen coverage. The particular benefit of this method is that it gives direct access to the role and energetics of the different potential local hydrogen adsorption sites.

We have chosen to resolve the characteristics of adsorption as a function of θ_H in contrast to commonly employed single-hydrogen adsorption, as there have been indications that the strength of adsorption is greatly affected by the total H-saturation of the surface[28]. By including θ_S and the adsorption site as additional variables, we strive for a comprehensive atomistic picture of the structure-property relations of H-adsorption on the various plausible 2H-MoS_2 surfaces. Additionally, the employed multilayer 3D-periodic approach provides new insight into the behavior of stacked MoS_2-edges, in contrast to the previously much reported semi-infinite 1D stripe model[13,28,32,37–40].

As such, this article conveys an exceptionally broad and systematical analysis of the inherent catalytic activity of MoS_2 with respect to HER. Indeed, the performed DFT-calculations show that of the many possible adsorption sites on the MoS_2-edges only a few exhibit catalytically preferential ΔG_H-values. The specific activities are further observed to depend heavily on the S-coverage, suggesting that not only the high relative abundance of edges in the prepared catalyst is enough for superior performance, but that the degree of S-saturation and the arrangement of the terminating S-atoms are equally important factors that need to be considered. Finally, it is concluded that a local activation of the 2H-MoS_2 basal plane is possible via vacancy inducing. Adsorption at the formed hollow sites is observed to be consistently thermoneutral in nature, thus suggesting optimal HER-performance. This finding is further supported by previous studies[18,21,33].

2 Methods

2.1 Computational details

All of the DFT-calculations in this work were conducted using the CP2K/Quickstep quantum chemistry package[41,42]. The hybrid Gaussian and plane waves method (GPW) was used with a plane wave energy cutoff of 550 Ry. The generalized gradient approximation (GGA) was applied using with the Perdew-Burke-Ernzerhof exchange-correlation functional[43] (PBE). The van der Waals dispersion interactions were taken into account by invoking the DFT-D3(BJ) method by Grimme *et al.* with Becke-Johnson damping[44,45]. The Kohn-Sham orbitals of the valence states were expanded in molecularly optimized double-ζ Gaussian basis sets[46], while the ionic cores were represented by Goedecker-Teter-Hutter (GTH) pseudopotentials[47–49]. The Kohn-Sham equations were solved using the orbital transformation (OT)[50] method and the DIIS minimizer (Pulay-mixing)[51]. The defined convergence criterion for the energy was $2.7 \times 10^{-5}\,eV$ and the structures were optimized using the Broyden-Fletcher-Goldfarb-Shanno (BFGS) algorithm[52–55] until the force on any atom was less than $0.023\,eV\,Å^{-1}$. 3D periodic boundary conditions were employed when solving the Poisson equation of the electrostatic potential.

2.2 Structures

2.2.1 Edge configurations

The studied 2H-MoS_2-edge configurations were constructed in accordance with the systems reported by Lauritsen *et al.*[56], along with the same θ_S assignment convention, i.e.

$$\theta_S = \frac{n_S}{2L_x}, \tag{1}$$

where L_x and n_S denote the edge length in terms of the number of Mo-atoms and the number of terminal S-atoms, respectively. Figure 1 displays the specific structures of the modeled edges as well as the probed adsorption sites. Henceforth, the specific edge-types will be referenced according to the convention "X-θ_S", where X is either Mo or S.

The lattice parameters were optimized by generating a set of trial systems with varying Mo-Mo (a), S-S (t) and interlayer separations ($c/2$), and calculating the respective total energies. Hence, the minimum energy parameters for the 2H-MoS_2 polytype were obtained as $a = 3.14\,Å$, $t = 3.15\,Å$ and $c/2 = 6.06\,Å$, respectively (Figure S1). This is in reasonable accordance with experimentally obtained results ($a \approx 3.15\,Å$, $c/2 \approx 6.15\,Å$)[19,57–59]. The supercells used in the H-adsorption calculations consist of

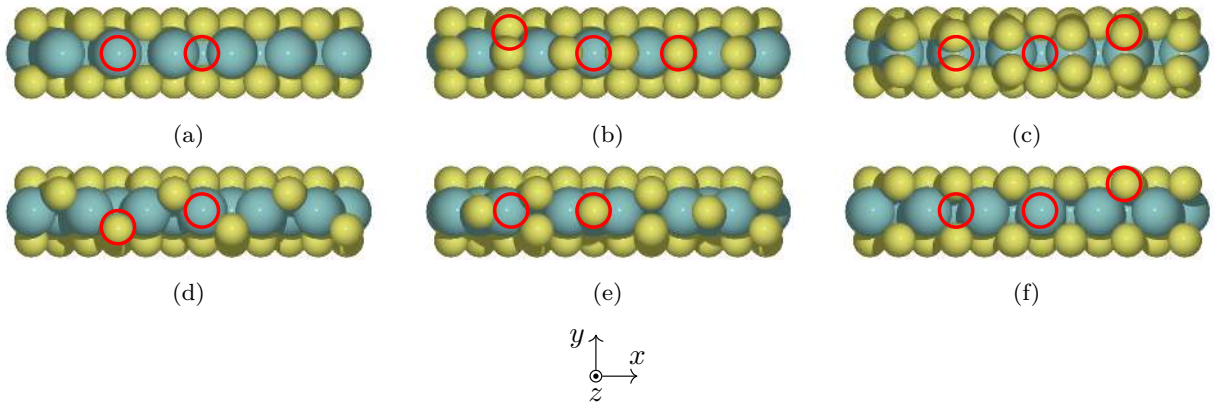

Fig. 1 Modeled Mo- and S-edges, adapted from[56]. Cyan and yellow spheres correspond to Mo and S, respectively. (a) Mo-0; adsorption sites from left to right: top, bridge. (b) Mo-50; bridge_1, bridge_2, top. (c) Mo-100; bridge, hollow, top. (d) S-50; top, bridge. (e) S-75; hollow, top. (f) S-100; bridge, hollow, top.

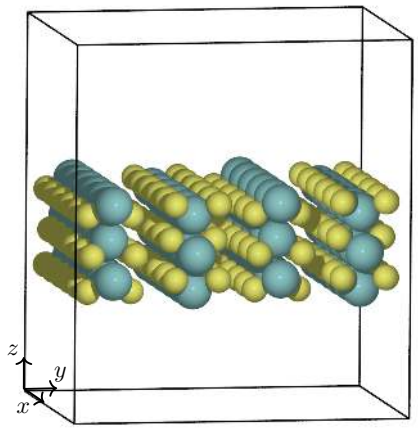

Fig. 2 Example of a geometry optimized edge-configuration with alternating S-100 and Mo-0 edges in the xy-plane.

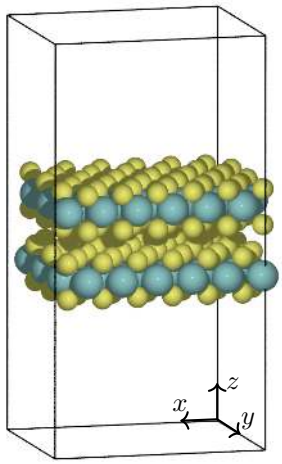

Fig. 3 Modeled geometry optimized bilayer 2H-MoS_2 basal plane.

four vertically aligned MoS_2 layers, stacked in the y-direction with 6×3 MoS_2-units in the xz-plane, totaling 72 and 144 Mo- and S-atoms, respectively. Due to the antiparallell AB-type stacking of 2H-MoS_2, the edge-surfaces of our configurations consist of alternating Mo- and S-edges, and thus every other layer represents the edge-type under investigation, while the remaining layers are "placeholders", ensuring the proper geometry of the whole system. When studying Mo-edges, the auxiliary S-edges were constructed to have $\theta_S = 100\,\%$, while for S-edges auxiliary Mo-0 was used. The choices of the specific placeholder edges were completely arbitrary and should not affect the final results as the atomic motion of these edges were fully constrained. An example of an optimized edge-configuration with alternating Mo-0 and S-100 edge-terminations is displayed in Figure 2.

For all edge-configurations, approximately 10 Å of vacuum was added both above and below the slabs in the z-direction, resulting in a total supercell volume of $18.84 \times 24.24 \times 27.15\,\text{Å}^3$. Thus, our edge-systems consist of 2D-infinite, three MoS_2-units thick surface slabs, reoccurring periodically in the z-direction.

2.2.2 Basal plane

The constructed 2H-MoS_2 basal plane configurations consist of two layers stacked in the z-direction, each containing 6×6 MoS_2-units and thus totaling 72 Mo-atoms and 144 S-atoms (Figure 3).

The defined lattice parameters are identical to the edge configurations and the supercell volume is $18.84 \times 16.32 \times 36.36\,\text{Å}^3$, including approximately 13 Å vacuum above and below the exposed basal planes along the z-coordinate. The S-deficient configurations were constructed by simply removing a certain amount of surface S-atoms to create either monovacancies (V_S) or divacancies (V_{S_2}). The vacancies were positioned such that an as good as uniform distribution was achieved. The sulfur deficiency is denoted by $\delta_S = 1 - \theta_S$, and signifies the fraction of S-atoms that have been removed from the pristine surface. In this context, θ_S has been modified to apply for the basal plane by replacing $2L_x$ in equation (1) by the total number of Mo-atoms per monolayer ($L_xL_y = 36$). The actual number of vacancies, however, naturally depends on the nature of the vacancy (at a given δ_S the number of monovacancies is twice the number of divacancies). Examples of geometry optimized vacancy-containing 2H-MoS_2 basal planes with an S-deficiency of $\delta_S = 16.7\,\%$ are presented in Figure 4. In

addition to this δ_S, we have studied the S-deficiencies 5.6 % and 11.1 %, respectively corresponding to 2 (1) and 4 (2) monovacancies (divacancies) per simulation cell.

2.3 Calculations

2.3.1 Stability estimation

The stability of the investigated 2H-MoS_2 configurations has been assessed by estimating the relative energies of formation per MoS_2-unit (edges) or per formed vacancy (S-deficient basal planes). This is given by

$$\Delta E_f = \frac{1}{n_i}\left[E_{sys} - (E_{ref} + \Delta n_S E_{S,ref})\right], \quad (2)$$

where E_{sys} is the energy of the investigated system and the reference energy $E_{ref} + \Delta n_S E_{S,ref}$ is defined as the energy of the pristine 2H-MoS_2 basal plane configuration, adjusted to have an equal amount of S-atoms as the target system (number of Mo-atoms is constant throughout the calculations). Δn_S denotes this excess/shortage of S-atoms between the system and the reference, and $i = MoS_2$ or V_{S_x} depending on the considered system. Considering the sulfiding atmosphere used during synthesis, we employed an atomic reference energy for sulfur in accordance with $E_{S,ref} = E_{H_2S} - E_{H_2}$. This choice for the reference energy has also been used by Byskov *et al.*[37] as well as Bollinger *et al.*[38]. For a more rigorous analysis of the stability, the variable values of the chemical potential of sulfur can be taken into account as done for example in [60]. Our intention here is to obtain a rough estimate of the stability trends when e.g. increasing the sulfur saturation of a certain edge-type.

2.3.2 Hydrogen adsorption

The hydrogen adsorption characteristics of the studied systems were analyzed by calculating the average free energy of adsorption as a function of θ_H and interpreting the results on the basis of the Sabatier principle. The hydrogen coverage is defined by

$$\theta_H = \frac{n_H}{n_{site}}, \quad (3)$$

where n_H is the number of adsorbed hydrogen intermediates and n_{site} quantifies the total number of specific adsorption sites on the studied surface to which the adsorption is conducted. The adsorption energy (ΔE_H) was calculated according to

$$\Delta E_H = \frac{1}{n_H}\left[E_{MoS_2+nH} - \left(E_{MoS_2} + \frac{n_H}{2}E_{H_2}\right)\right], \quad (4)$$

where E_{MoS_2+nH} and E_{MoS_2} are the energies of the final configuration and the hydrogen-free initial configuration, respectively[61]. The free energy is related to the adsorption energy by

$$\Delta G_H = \Delta E_H + \Delta E_{ZPE} - T\Delta S_H, \quad (5)$$

where $\Delta E_{ZPE} = E^H_{ZPE} - \frac{1}{2}E^{H_2}_{ZPE}$ and $\Delta S_H = S^\circ_H - \frac{1}{2}S^\circ_{H_2}$ are the change in the zero point energy and entropy between the adsorbed state H* and the gas phase H_2, respectively. The contribution of these terms is assumed to be constant (≈ 0.29 eV), as proposed by Hinnemann *et al.*[6] (see supplementary information).

The affinity of specific sites towards hydrogen adsorption was probed by constraining the movement of the approaching H-atoms to the vertical z-coordinate, perpendicular to the surface under investigation. For improved convergence, also the auxiliary edges and the bottom layers of the systems were constrained (Figure 5). For all system types and adsorption sites, configurations with increasing θ_H were constructed and a geometry optimization was conducted within the limits of the employed constraints. The incremental increasing of θ_H was realized by uniformly positioning hydrogen atoms above the vacant adsorption sites so that initially every other site was incrementally occupied, and when a coverage of 0.5 ML had been reached, the remaining adjacent sites were filled.

3 Results

3.1 Edge configurations

3.1.1 Adsorption studies

The free energies of hydrogen adsorption on to 2H-MoS_2 edges are generally observed to increase, i.e. the adsorption weakens, as θ_H increases (Figure 6). This trend is in good accordance with previously reported results for both pristine and doped 2H-MoS_2[32], as well as with other transition metal dichalcogenides and phosphides in general[28,40].

As we have employed geometry-constrained calculations for the precise probing of specific adsorption sites, we expect our ΔG_H-values to take slightly higher values than would be observed in unconstrained calculations. This has to be taken into account when comparing individual ΔG_H-values to the literature. However, we will mainly restrict the analysis of the results to the observed trends and relative differences. As Figure 6 suggests, the various adsorption sites and edges exhibit very different affinities towards H-adsorption, thus indicating that only certain sites on certain edge-configurations are responsible for the electrocatalytic activity of 2H-MoS_2. On the Mo-edge, the bare Mo-0 surface binds hydrogen strongly ($\Delta G_H < 0$ eV), and of the investigated sites adsorption at the Mo-Mo-bridge is seen to yield the most stable Mo-H bonds. Thus, even though adsorption at the top-site would yield close to thermoneutral adsorption, especially at high θ_H, H-adsorption is most likely more prone to occur at the competing Mo-Mo-bridge site, as a larger decrease in energy can thus be achieved. The remaining Mo-edges and sites bind hydrogen more weakly, with the Mo-50 top- (low H-coverage) and bridge$_1$-sites (all H-coverages) providing for the most thermoneutral, and thus most promising, adsorption behavior. Adsorption on the other sites/edges is less likely to occur due to very weak adsorbate/adsorbent-interaction.

For the studied sites on the S-edges, mostly weak adsorption is observed. Only adsorption to the top-site on the fully-sulfided S-edge exhibits thermoneutral bonding, especially at intermediate H-coverages. In addition, the S-100 bridge-site shows adsorption relatively close to the thermoneutral limit (~ 0.3 eV). Adsorption to the other sites/edges is less likely to occur, as is indicated by the very weak Mo-H bonding. The site-specificity of hydrogen adsorption is clearly illustrated by the behavior of ΔG_H on the S-100 edge, where the hollow site displays signifi-

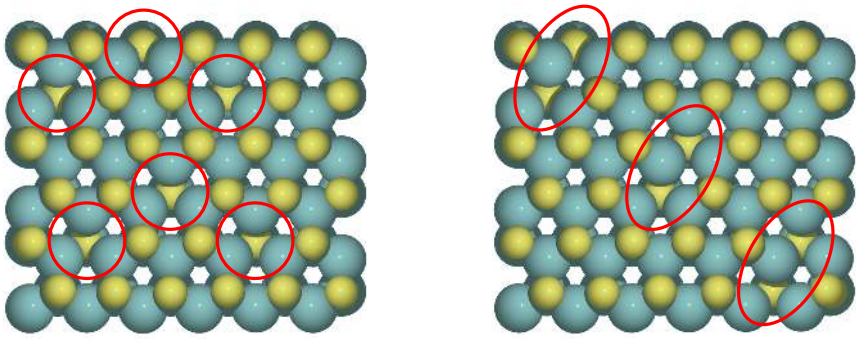

(a) (b)

Fig. 4 Examples of geometry optimized S-deficient 2H-MoS_2 basal planes with $\delta_S = 16.7\,\%$. (a) System with 6 monovacancies (V_S, indicated by red circles). (b) System with 3 divacancies (V_{S_2}, indicated by red ellipses).

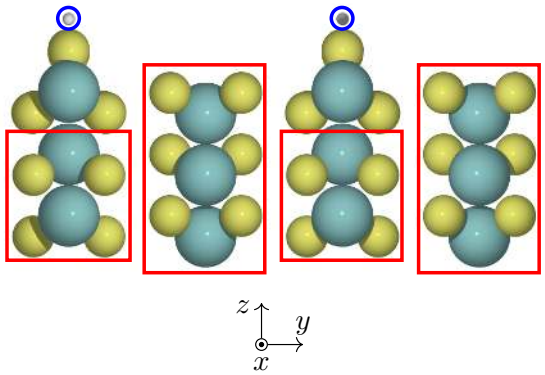

Fig. 5 Illustration of the applied constraints (Mo-50 edge as an example). The movement of atoms within the blue circles (H) was constrained to the vertical z-coordinate directly above the studied adsorption sites (in this case Mo-50 top-site). The positions of the Mo- and S-atoms within the red rectangles were fully fixed, while the remainder of the system was allowed to relax freely.

cantly lower affinity towards hydrogen than the bridge and top-sites ($\Delta\Delta G_H \approx 0.6 \ldots 1.0\,\text{eV}$ depending on θ_H). The same is seen on the Mo-50 edge for adsorption to the bridge$_2$ site. For the remaining edges, the differences between sites are more subtle ($\Delta\Delta G_H < 0.5\,\text{eV}$), but still clearly noticeable.

As mentioned, Figure 6 shows that increasing θ_H generally weakens the strength of adsorption. This can be understood in simple terms by an increasing repulsion between H-adsorbates. However, as adsorption occurs, the positions of nearby Mo- and S-atoms are in addition perturbed in a way that minimizes the energy of the new adsorbate/adsorbent-system. The rearrangement becomes more hindered as more hydrogen adsorbs due to less degrees of freedom, which destabilizes the system. This provides an additional explanation for the increasing ΔG_H and is in agreement with results presented by Tsai *et al.*[28,32]. However, the opposite trend where increasing θ_H in fact is seen to significantly strengthen the adsorption, was surprisingly observed for the edge/site combinations presented in Figure 7.

For the Mo-100 (bridge/top) and S-75 (hollow/top) edges, in which this decreasing ΔG_H trend was observed, it was seen that the adsorption of hydrogen is coupled with significant surface re-

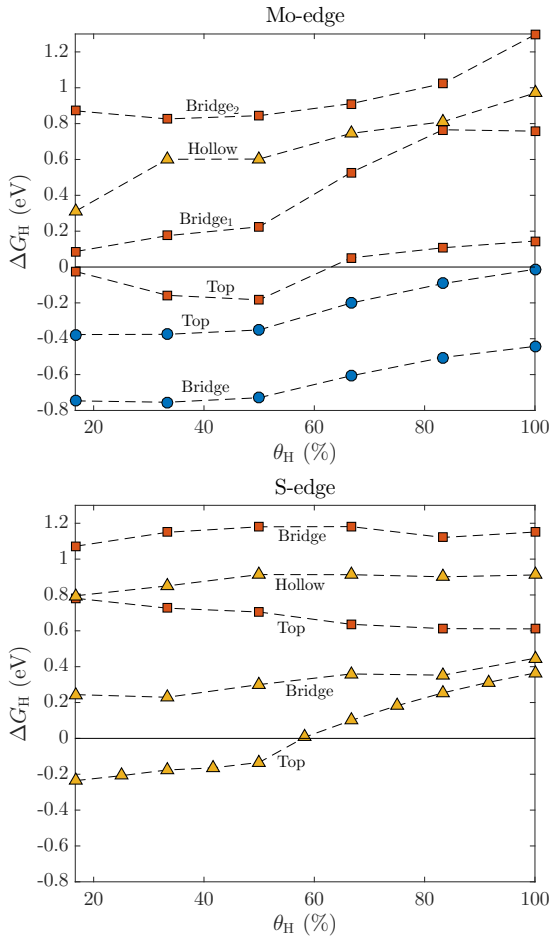

Fig. 6 Adsorption free energy as a function of hydrogen coverage for the studied edge-configurations. The θ_S-values of 0 %, 50 % and 100 % are indicated by blue circles, orange squares and yellow triangles, respectively.

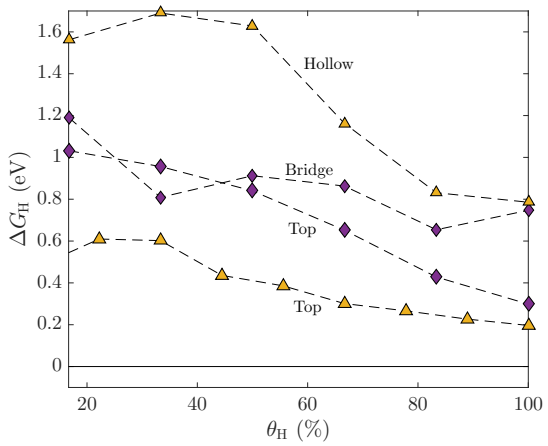

Fig. 7 Adsorption free energy as a function of hydrogen coverage for configurations in which an incremental strengthening of the hydrogen adsorption was observed with increasing θ_H. The yellow triangles designate the S-75 edge, while the blue rhombi correspond to the Mo-100 edge.

arrangements, mostly affecting the terminal S-atoms. Specifically, common for all cases is the splitting of the dimerized S_2-bridges, illustrated in Figure 8. The H-adsorption induced splitting of S_2-dimers has also been observed by Byskov *et al.*[37] for Co-doped MoS_2 as well as Bollinger *et al.*[38] for pristine MoS_2, while Tsai *et al.*[39], has reported similar behavior in the context of 2H-MoS_2 interactions with support materials. They argue that even though the barrier for the splitting is significant ($\Delta E \approx 0.8\,\mathrm{eV}$), the formation of a strong, singly coordinated S-H bond balances the energy cost and ultimately leads to an overall stabilization of the system.

The site-specific H-adsorption on to 2H-MoS_2 edges effectively illustrates the complexity of this type of material. The structural response of the surface is heavily site- and edge-dependent, and hence significantly varying adsorption strengths and trends are observed. Moreover, the S-saturation is seen to play a key role in determining the adsorption characteristics of either edge. Further illustrations of the observed adsorption induced reorganizations are given in the supplementary information (Figures S2 and S3).

3.1.2 Formation energy

In estimating the formation energies (Equation 2) of the edge configurations, all possible permutations containing one certain type of S-edge and Mo-edge (alternatingly stacked as described in Section 2.2) were considered, thus resulting in 9 different multilayer systems. The relative stabilities when compared to the thermodynamically favored basal plane are shown in Table 1.

All modeled edge structures are seen to be less stable than the basal plane ($\Delta E_f > 0$), which is in accordance with the general consensus. Further, it is seen that increasing θ_S of both edges results in stabilization of the systems. The S-coverage of the Mo-edge is observed to greatly influence the overall stability when $\theta_S(\mathrm{Mo}) \leq 50\,\%$, but at higher values the stability is approximately constant for a fixed $\theta_S(\mathrm{S})$. Increasing the S-saturation of the S-edge on the other hand shows a decreasing trend in ΔE_f in the whole studied θ_S-interval, however the relative differences are

Table 1 Relative energies of formation of the modeled edge structures ($\theta_H = 0$), normalized per MoS_2 unit. The 2H-MoS_2 basal plane is taken as the reference system ($\Delta E_f \equiv 0\,\mathrm{eV}$, $Mo_{72}S_{144}$). All studied supercells contain two Mo- and S-edges of the same type, with the respective S-coverages denoted by $\theta_S(\mathrm{Mo})$ and $\theta_S(\mathrm{S})$.

ΔE_f (eV)		$\theta_S(\mathrm{S})$ (%)		
		50	75	100
$\theta_S(\mathrm{Mo})$ (%)	0	1.77	1.73	1.57
	50	1.42	1.36	1.23
	100	1.42	1.36	1.21

not as pronounced as between $\theta_S(\mathrm{Mo}) = 0\,\%$ and $\theta_S(\mathrm{Mo}) = 50\,\%$. This estimation is qualitatively consistent with the computational results presented by Byskov *et al.*[37], which demonstrate that the coordinatively unsaturated Mo-atoms in the Mo-0 configuration are thermodynamically very unfavorable, while increasing the coverage to 50 % or 100 % allows the edge Mo-atoms to reach full six-fold coordination and hence higher stability. The comparable stability of the Mo-50 edge with the Mo-100 edge can be understood in terms of significant reconstruction (shift of S-atoms by half a lattice constant), which allows the six-fold S-coordination also on the half-saturated Mo-edge. Experimental support for these claims have been provided by Hansen *et al.*[62] by means of high-resolution scanning transmission electron microscopy.

Furthermore, the clearer differences in the relative stability of S-edges throughout the studied θ_S regime is due to the S-100 configuration being the only edge with optimally coordinated Mo-atoms. Thus, decreasing the S-coverage on the S-edge instantly yields coordinatively unsaturated Mo-atoms, as no similar reconstruction as seen for Mo-50 occurs, which would maintain the six-fold coordination of Mo at the edge. Similar conclusions have been drawn by Bollinger *et al.*[38]. More rigorous stability estimations with the inclusion of the effects of the sulfur chemical potential (μ_S) have been conducted by Schweiger *et al.*[60]. When the limit of low μ_S, relevant at the sulfiding conditions during synthesis, is considered, the qualitative conclusion of their studies regarding the relative stabilities of the different 2H-MoS_2 edges is the same as presented herein. Thus, our 0 K stability assessment can be considered suitable as a first approximation.

3.2 Sulfur-deficient basal plane

3.2.1 Adsorption studies

The activating effect of inducing S-vacancies in the 2H-MoS_2 basal plane has been studied by Li *et al.*[18] as well as Ouyang *et al.*[33]. We have investigated this further by inducing both single-atom vacancies (V_S) and divacancies (V_{S_2}) to a pristine bilayer 2H-MoS_2 basal plane ($Mo_{72}S_{144}$), and employing H-adsorption calculations as a function of θ_H. Initially, hydrogen is adsorbed into the vacant sites, which after complete occupation is followed by adsorption to adjacent top-sites. The obtained ΔG_H-trends are presented in Figure 9.

Compared to the ΔG_H-values obtained for adsorption onto the pristine 2H-MoS_2 basal plane ($\Delta G_H \approx 2.0\,\mathrm{eV}$), the adsorption energetics is significantly improved as a result of inducing vacancies. However, the most prominent improvement applies only for adsorption to the actual vacancy-sites ($\Delta G_H \approx -0.2\,\mathrm{eV} \ldots 0\,\mathrm{eV}$),

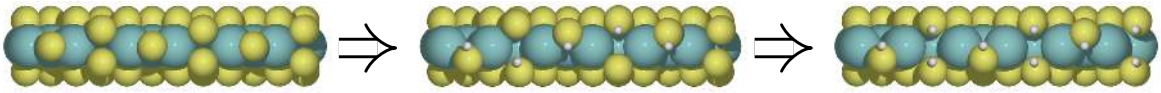

Fig. 8 Example of observed major surface reorganization on the S-75 edge. The most evident feature is the splitting of the terminating S_2-dimers.

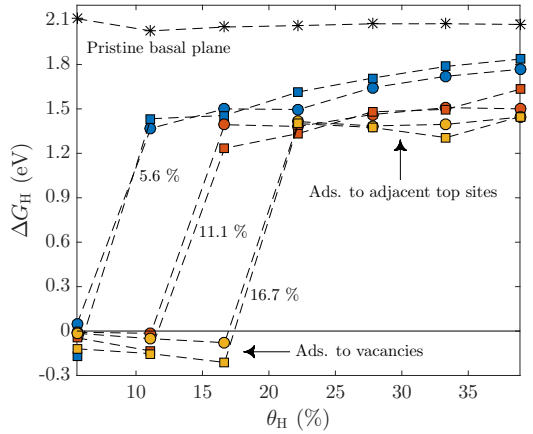

Fig. 9 H-adsorption free energies for S-deficient basal planes as a function of θ_H. $\delta_S = 5.6\,\%$, $11.1\,\%$ and $16.7\,\%$ corresponds to 2 (1), 4 (2) and 6 (3) monovacancies (divacancies) per simulation cell, respectively. The circles denote monovacancies and squares divacancies. The free energy of adsorption on the pristine 2H-MoS_2 basal plane is given as a reference (black stars). The approximately thermoneutral values are associated with H-adsorption to vacant S-sites, while the high positive ($\Delta G_H > 1\,eV$) energies correspond to adsorption to adjacent top-sites.

while adsorption to adjacent top-sites is only slightly improved ($\Delta G_H \approx 1.2\,eV \ldots 1.8\,eV$). Thus, inducing vacancies tunes the electronic structure of the basal plane mainly locally, and to achieve comprehensive activation a large concentration of vacancies is therefore needed. This is problematic, as an increasing amount of vacancies can be expected to result in destabilized configurations, as will be seen in the following subsection. The thermoneutral adsorption free energies of adsorption to monovacancies and the locality of the activating effect is in seamless agreement with the results of Li *et al.*[18], who ascribed the improved activity to result from the formation of localized gap-states in close proximity to the Fermi level of the material.

According to the presented data, a larger δ_S results in slightly higher activation, i.e. strengthened adsorption, at sites adjacent to the vacancies (differences are $\sim 0.1\,eV$). Additionally, it is noted that basal planes with divacancies yield slightly stronger adsorption than corresponding systems with monovacancies when hydrogen adsorbs to vacant sites ($\Delta\Delta G_H \approx 0.1 \ldots 0.2\,eV$). On the other hand when adsorption occurs to adjacent top-sites, no as clear differences between mono- and divacancy containing systems can be observed, especially in the case of the systems with $\delta_S = 11.1\,\%$ and $16.7\,\%$. Interestingly, for $\delta_S = 5.6\,\%$ a reversal of the trend is seen, where in fact on-top adsorption on the monovacancy containing basal plane yields slightly lower ΔG_H-values than the corresponding system with divacancies. The observed slightly stronger adsorption to divacant sites compared to monovacancies is in accordance with the findings of Ouyang *et al.*[33], who report a strengthening of $0.12\,eV$ in the H-adsorption between these configurations.

Similarly as for adsorption on edge-configurations, ΔG_H is seen to increase with an increasing θ_H upon adsorption to adjacent top-sites. As negligible surface-reconstruction was observed for these S-deficient systems upon vacancy inducing and H-adsorption, the weakened adsorption can be expected to result mainly from the repulsive adsorbent interactions induced by an increased crowding of the surface. However, at low θ_H (adsorption to vacancies) the adsorption is seen to strengthen slightly as the occupation of the vacancies increases. This can be understood by a stabilization of the energetically unfavorable hollow sites with undercoordinated Mo-atoms.

3.2.2 Formation energy

The energetics of vacancy-formation has been estimated in accordance with Equation 2, and the results are shown tabulated in Table 2. Not surprisingly, it is seen that inducing vacancies requires a net input of energy, hence demonstrating their thermodynamical unfavorability compared to the pristine basal plane.

Table 2 Relative energy-cost per formed vacancy (V_S or V_{S_2}) for the studied S-deficient systems. Again, the pristine 2H-MoS_2 basal plane configuration is used as the reference system.

δ_S (%)	ΔE_f (eV)	
	V_S	V_{S_2}
5.6	2.72	5.38
11.1	2.76	5.42
16.7	2.77	5.50

The vacancy formation energies are observed to be very high, thus indicating that their intrinsic thermal formation is unlikely. Hence, vacancies in the 2H-MoS_2 basal plane are metastable in nature and have to be induced by external means, e.g. argon plasma sputtering[18]. Interestingly, our results suggest that if few vacancies are formed at the surface ($\delta_S \leq 16.7\,\%$), they tend to form rather pairs (that is, divacancies) than stay farther from each other as two isolated monovacancies, i.e. $\Delta E_f(V_{S_2}) < 2 \cdot \Delta E_f(V_S)$. Even though the differences are rather small ($-0.06\,eV$, $-0.10\,eV$ and $-0.04\,eV$), already the observation that the energetic cost of forming divacancies is approximately equal to forming monovacancies can intuitively be regarded as rather surprising. Nevertheless, this behavior is in line with results reported by Le *et al.*[63] as well as Sensoy *et al.*[64]. In the latter work it is shown that the defect-induced lattice reorganization in the 2H-MoS_2 basal plane is very small and local, and that the interaction between isolated monovacancies is negligible. Basing their conclusions on nudged elastic band (NEB) calculations showing very high monovacancy

diffusion barriers ($\sim 2.2\,\mathrm{eV}$), it is argued that the pairing of vacancies is unlikely, even though this might result in slightly lowered energies. Furthermore, the formation energies of neutral monovacancies and divacancies are determined to be approximately $2.6\,\mathrm{eV}$ and $5.2\,\mathrm{eV}$, in excellent agreement with our calculations. The formation of monovacancies in the basal plane of MoS_2 has been estimated also by Byskov *et al.*[37] using a similar methodology, and a value of approximately $2.3\,\mathrm{eV}$ is reported, which is in moderate agreement with the results presented herein.

Feng *et al.*[65] and Komsa and Krasheninnikov[66] have carried out computations on the monovacancy formation on 2H-MoS_2 basal planes with the inclusion of the sulfur chemical potential. In the S-rich limit (small μ_S) it is demonstrated that the formation energy of monovacancies ranges between approximately $2.5\,\mathrm{eV}$ and $3.0\,\mathrm{eV}$, depending on the position of the MoS_2 Fermi level. Thus, it is concluded that our estimation neglecting the chemical potential is reasonable as a first order approximation also in the case of S-deficient basal planes.

4 Discussion

The main result of the presented research is that the hydrogen adsorption characteristics on the studied 2H-MoS_2 surfaces are far from uniform. Indeed, significant variations and site-specificity are observed as a function of edge sulfur saturation and hydrogen coverage for both vertically aligned multilayer edge-configurations as well as vacancy containing basal planes. Most notably, the complex structural response of the systems upon H-adsorption efficiently demonstrate the dynamic nature of a real catalyst, indicating that the surface geometry of the material is most likely significantly perturbed from the equilibrium structure during operating conditions in electrochemical devices. This is seen to be especially true for those studied systems containing terminal S_2-dimers, which split as a result of H-adsorption. The detailed structural reconstruction is observed to be intimately linked with the predicted activity of the material, particularly that minor reorganization induced by H-adsorption results in incrementally weakened adsorption, while major perturbations are coupled to an apparent activation of the material. In the future, the H-coverage analysis should be extended to fully relaxed structures, which would capture the non-local, long-range phenomena that can affect the reconstruction and the ensuing adsorption energies.

It is interesting to consider the effects of hydrogen co-adsorption, by which is meant the simultaneous or subsequent adsorption of hydrogen to sites of different type on the same surface, on the energetics. For example, it is plausible that the adsorption of hydrogen to a certain site alters the electronic structure of the material in a way that results in the activation of some other nearby site. Similar behavior is indeed observed in the present study for hydrogen adsorption to edge sites of the same type (single-site adsorption). For example, adsorption to top-sites on Mo-0 and S-100 edges results in activation via arising repulsive and straining forces, which weaken the adsorption of subsequent species. The thermoneutral limit is seen to be reached at half and full coverage for S-100 and Mo-0 edges, respectively, at which point the configurations may be considered activated and operational for HER catalysis. On the other hand, activation via strengthened adsorption is observed for top-site adsorption on S-75 and Mo-100 edges. In this case initial adsorption of hydrogen induces significant surface restructuring, which perturbs nearby sites such that subsequently adsorbed hydrogens are bound more strongly with ΔG_H-values closer to the thermoneutral limit.

On this basis it can be suggested that also co-adsorption may have significant activating effects. This phenomenon is well known to exist for platinum, where underpotential- and overpotential deposited hydrogen intermediates (H_{upd}, H_{opd}) have been identified[67,68]. The species have been proposed to occupy different sites on the Pt-surface, and that the interaction between them plays a key role in determining the HER kinetics. In particular, H_{upd}, which is suggested to bind strongly to hollow sites, alters the adsorption energy of H_{opd}-species, which are considered to adsorb to top-sites, via repulsive interactions. This results in a significant activation of the overpotential deposited hydrogen, which hence serves as the reactive intermediate of the HER on Pt (cf. single-site adsorption results for Mo-0/top and S-100/top). The investigation of co-adsorption on 2H-MoS_2 is an interesting topic to consider in future research.

In general, our results underline that the development of effective MoS_2-based HER-catalysts requires not only an optimization of the relative edge-to-bulk ratio, but also a detailed engineering of the degree of S-saturation, so as to achieve systems in which the most active edge types and terminations are comprehensively exposed. A naturally arising question in relation to this is of course whether such a detailed tailoring of the catalyst is possible in reality. Lauritsen *et al.*[56] have demonstrated that the degree of S-saturation is highly dependent on the size of the synthesized MoS_2 clusters. Also, the morphology of the clusters has been shown to be very sensitive to changes in the conditions applied during synthesis (μ_S)[60,69]. This has direct implications on the Mo-to-S edge ratio, and thus on the resulting activity of the material. As such, it is seen that by controlling the size distribution of synthesized 2H-MoS_2 clusters, as well as optimally tuning the processing conditions, the structural and therefore catalytical properties of the material can be accurately tuned. This implies that the degree of structural tailoring proposed herein to be necessary for the rigorous optimization of MoS_2 is experimentally manageable.

Furthermore, the introduction of S-vacancies into the 2H-MoS_2 basal plane for comprehensive activation of the material as a whole has been shown to be achievable by e.g. Ar-plasma treatment, with subsequent electrochemical measurements of the as prepared catalyst yielding results qualitatively in line with computational predictions[18]. However, even though adsorption to vacant sites exhibits thermoneutral characteristics comparable, or even superior, to Pt, the electrochemical measurements show that cathodic polarization has to be conducted to substantially higher overpotentials to reach similar HER current densities, i.e. reaction kinetics, as for Pt ($10\,\mathrm{mA\,cm^{-2}}$ at $-250\,\mathrm{mV}$ and $-59\,\mathrm{mV}$ for vacancy-containing MoS_2 and Pt, respectively). This is a commonly observed result for other modeled catalysts as well (e.g. results presented in[11,17,19,20] for other pristine and modified MoS_2-based systems).

The encountered discrepancies[11,17–20] between theory and ex-

periments demonstrate the drawbacks of using ΔG_H as a sole descriptor in the modeling of novel HER electrocatalysts, as the overall process is clearly very complex and dependent on several other parameters than just H-adsorption. Nevertheless, if a fast screening of materials properties is desired, the descriptor based approach serves as to give directive results, aiding e.g. in narrowing down a set of potential catalysts to a few most promising ones, for which more accurate calculations/experiments can then be conducted. Additionally, if fast screening of several systems is to be conducted with concurrent consideration of additional parameters, such as the hydrogen coverage and/or site specificity as in this study, further coarse-graining to decrease the degrees of freedom is necessary for a systematical treatise. As reasoned previously, the approach chosen here comes with some artefacts, as the applied constraints yield absolute adsorption energies somewhat higher than obtained in similar measurements performed by others[20,39]. Nevertheless, this method enables the precise probing of individual adsorption sites as a function of H-coverage and yields qualitatively correct trends, as the same constraints are consistently employed in all calculations.

5 Conclusions

In the present work we have employed DFT-calculations to systematically and comprehensively study the atomistic details of hydrogen adsorption on various 2H-MoS_2 surfaces. The adsorption characteristics have been resolved as a function of hydrogen coverage, degree of sulfur saturation at the studied surface, as well as the potential adsorption sites. The activity of the studied configurations has been assessed on the basis of the ΔG_H-descriptor and the Sabatier principle. Additionally, the relative stabilities of the systems have been estimated by calculating the corresponding energies of formation.

The hydrogen adsorption on 2H-MoS_2 edges is shown to be heavily dependent on the edge-type, and particularly on the degree of sulfur coverage as well as on the adsorption site to which adsorption occurs. In general, a weakening of the adsorption strength is observed with increasing H-coverage, well in line with previous findings. However, certain systems involving terminal S_2-dimers at the edges exhibit the opposite trend, with significant adsorption induced activation occurring coupled with major surface reconstructions (splitting of the S_2-dimers). Further, inducing sulfur vacancies in the otherwise inert 2H-MoS_2 basal plane is observed to remarkably improve the adsorption, which successfully corroborates previous studies. However, the activating effect is seen to be exclusive to the vacant S-sites, as adsorption to adjacent top-sites is negligibly affected compared to the pristine surface.

The performed calculations effectively demonstrate the complex and rich structure-property relationships of H-adsorption on 2H-MoS_2. Based on the results it can be concluded that detailed reconstructions of the atomic and electronic structure upon H-adsorption and vacancy-inducing are important phenomena that determine the dynamic catalytic behavior of MoS_2 in its various configurations. As the atomistic picture of the activity and stability of the studied material is highly dependent on a multitude of interrelated variable parameters, determined by e.g. the synthesis environment and the working conditions, MoS_2 constitutes an ideal case for machine learning methods. In upcoming research we will utilize the herein generated data on 2H-MoS_2, as well as results obtained in parallel to this study for transition metal doped configurations, for the training of predictive algorithms by which the screening of novel HER-electrocatalysts could potentially be made significantly faster. We will also proceed to extend the obtained results with more detailed reaction calculations involving explicit modeling of the solvent, as well as expand the consideration to encompass other materials families, such as transition metal phosphides, and other electrochemical reactions relevant in energy conversion and storage.

Acknowledgements

The work was supported by the European Union's Horizon 2020 research and innovation programme (CritCat Project, grant agreement No. 686053). The computing resources provided by CSC - IT Center for Scientific Computing, including the Grand Challenge project CritCat, are gratefully acknowledged.

Author contributions statement

R.K. performed all the calculations with assistance from N.H., as well as wrote the manuscript and analyzed the main results. M.H. and K.L. contributed to the interpretation of the results and the manuscript was reviewed by all authors.

Additional information

The authors declare no competing financial interests.

References

1 J. A. Turner, *Science*, 2004, **305**, 972–974.

2 G. Marbán and T. Valdés-Solís, *Int. J. Hydrogen Energy*, 2007, **32**, 1625–1637.

3 T. R. Cook, D. K. Dogutan, S. Y. Reece, Y. Surendranath, T. S. Teets and D. G. Nocera, *Chem. Rev.*, 2010, **110**, 6474–6502.

4 H. B. Gray, *Nat. Chem.*, 2009, **1**, 7.

5 P. C. Vesborg, B. Seger and I. Chorkendorff, *J. Phys. Chem. Lett.*, 2015, **6**, 951–957.

6 B. Hinnemann, P. G. Moses, J. Bonde, K. P. Jørgensen, J. H. Nielsen, S. Horch, I. Chorkendorff and J. K. Nørskov, *J. Am. Chem. Soc.*, 2005, **127**, 5308–5309.

7 D. Merki and X. Hu, *Energy Environ. Sci.*, 2011, **4**, 3878–3888.

8 J. D. Benck, T. R. Hellstern, J. Kibsgaard, P. Chakthranont and T. F. Jaramillo, *ACS Catal.*, 2014, **4**, 3957–3971.

9 J. Wilson and A. Yoffe, *Adv. Phys.*, 1969, **18**, 193–335.

10 T. F. Jaramillo, K. P. Jørgensen, J. Bonde, J. H. Nielsen, S. Horch and I. Chorkendorff, *Science*, 2007, **317**, 100–102.

11 J. Bonde, P. G. Moses, T. F. Jaramillo, J. K. Nørskov and I. Chorkendorff, *Farad. Discuss.*, 2009, **140**, 219–231.

12 A. B. Laursen, S. Kegnæs, S. Dahl and I. Chorkendorff, *Energy Environ. Sci.*, 2012, **5**, 5577–5591.

13 C. Tsai, K. Chan, F. Abild-Pedersen and J. K. Nørskov, *Phys. Chem. Chem. Phys.*, 2014, **16**, 13156–13164.

14 J. Kibsgaard, Z. Chen, B. N. Reinecke and T. F. Jaramillo, *Nat. Mater.*, 2012, **11**, 963–969.

15 J. Deng, W. Yuan, P. Ren, Y. Wang, D. Deng, Z. Zhang, X. Bao *et al.*, *RSC Advances*, 2014, **4**, 34733–34738.

16 M.-R. Gao, M. K. Chan and Y. Sun, *Nat. Commun.*, 2015, **6**, 1–8.

17 J. Deng, H. Li, J. Xiao, Y. Tu, D. Deng, H. Yang, H. Tian, J. Li, P. Ren and X. Bao, *Energy Environ. Sci.*, 2015, **8**, 1594–1601.

18 H. Li, C. Tsai, A. L. Koh, L. Cai, A. W. Contryman, A. H. Fragapane, J. Zhao, H. S. Han, H. C. Manoharan, F. Abild-Pedersen *et al.*, *Nat. Mater.*, 2016, **15**, 48–53.

19 B. Seo, G. Y. Jung, Y. J. Sa, H. Y. Jeong, J. Y. Cheon, J. H. Lee, H. Y. Kim, J. C. Kim, H. S. Shin, S. K. Kwak *et al.*, *ACS Nano*, 2015, **9**, 3728–3739.

20 H. Wang, C. Tsai, D. Kong, K. Chan, F. Abild-Pedersen, J. K. Nørskov and Y. Cui, *Nano Res.*, 2015, **8**, 566–575.

21 G. Ye, Y. Gong, J. Lin, B. Li, Y. He, S. T. Pantelides, W. Zhou, R. Vajtai and P. M. Ajayan, *Nano Lett.*, 2016, **16**, 1097–1103.

22 M. A. Lukowski, A. S. Daniel, F. Meng, A. Forticaux, L. Li and S. Jin, *J. Am. Chem. Soc.*, 2013, **135**, 10274–10277.

23 M. Mortazavi, C. Wang, J. Deng, V. B. Shenoy and N. V. Medhekar, *J. Power Sources*, 2014, **268**, 279–286.

24 Y. Li, H. Wang, L. Xie, Y. Liang, G. Hong and H. Dai, *J. Am. Chem. Soc.*, 2011, **133**, 7296–7299.

25 J. Greeley, T. F. Jaramillo, J. Bonde, I. Chorkendorff and J. K. Nørskov, *Nat. Mater.*, 2006, **5**, 909–913.

26 T. Liao, Z. Sun, C. Sun, S. X. Dou and D. J. Searles, *Sci. Rep.*, 2014, **4**, 1–7.

27 Z. Wang, Q. Chen and J. Wang, *J. Phys. Chem. C*, 2015, **119**, 4752–4758.

28 C. Tsai, K. Chan, J. K. Nørskov and F. Abild-Pedersen, *Surf. Sci.*, 2015, **640**, 133–140.

29 S. S. Chou, N. Sai, P. Lu, E. N. Coker, S. Liu, K. Artyushkova, T. S. Luk, B. Kaehr and C. J. Brinker, *Nat. Commun.*, 2015, **6**, 1–8.

30 G. Gao, Q. Sun and A. Du, *J. Phys. Chem. C*, 2016, **120**, 16761–16766.

31 X. Fan, S. Wang, Y. An and W. Lau, *J. Phys. Chem. C*, 2016, **120**, 1623–1632.

32 C. Tsai, K. Chan, J. K. Nørskov and F. Abild-Pedersen, *Catal. Sci. Technol.*, 2015, **5**, 246–253.

33 Y. Ouyang, C. Ling, Q. Chen, Z. Wang, L. Shi and J. Wang, *Chem. Mater.*, 2016, **28**, 4390–4396.

34 J. K. Nørskov, T. Bligaard, A. Logadottir, S. Bahn, L. B. Hansen, M. Bollinger, H. Bengaard, B. Hammer, Z. Sljivancanin, M. Mavrikakis *et al.*, *J. Catal.*, 2002, **209**, 275–278.

35 T. Bligaard, J. Nørskov, S. Dahl, J. Matthiesen, C. Christensen and J. Sehested, *J. Catal.*, 2004, **224**, 206–217.

36 J. K. Nørskov, T. Bligaard, A. Logadottir, J. Kitchin, J. G. Chen, S. Pandelov and U. Stimming, *J. Electrochem. Soc.*, 2005, **152**, J23–J26.

37 L. S. Byskov, J. K. Nørskov, B. S. Clausen and H. Topsøe, *J. Catal.*, 1999, **187**, 109–122.

38 M. Bollinger, K. W. Jacobsen and J. K. Nørskov, *Phys. Rev. B*, 2003, **67**, 085410.

39 C. Tsai, F. Abild-Pedersen and J. K. Nørskov, *Nano Lett.*, 2014, **14**, 1381–1387.

40 J. Kibsgaard, C. Tsai, K. Chan, J. D. Benck, J. K. Nørskov, F. Abild-Pedersen and T. F. Jaramillo, *Energy Environ. Sci.*, 2015, **8**, 3022–3029.

41 J. Hutter, M. Iannuzzi, F. Schiffmann and J. VandeVondele, *Wiley Interdiscip. Rev.: Comput. Mol. Sci.*, 2014, **4**, 15–25.

42 J. VandeVondele, M. Krack, F. Mohamed, M. Parrinello, T. Chassaing and J. Hutter, *Comput. Phys. Commun.*, 2005, **167**, 103–128.

43 J. P. Perdew, K. Burke and M. Ernzerhof, *Phys. Rev. Lett.*, 1996, **77**, 3865–3868.

44 S. Grimme, J. Antony, S. Ehrlich and H. Krieg, *J. Chem. Phys.*, 2010, **132**, 154104.

45 S. Grimme, S. Ehrlich and L. Goerigk, *J. Comput. Chem.*, 2011, **32**, 1456–1465.

46 J. VandeVondele and J. Hutter, *J. Chem. Phys.*, 2007, **127**, 114105.

47 S. Gœdecker, M. Teter and J. Hutter, *Phys. Rev. B*, 1996, **54**, 1703.

48 C. Hartwigsen, S. Gœdecker and J. Hutter, *Phys. Rev. B*, 1998, **58**, 3641.

49 M. Krack, *Theor. Chem. Acc.*, 2005, **114**, 145–152.

50 J. VandeVondele and J. Hutter, *J. Chem. Phys.*, 2003, **118**, 4365–4369.

51 P. Pulay, *Chem. Phys. Lett.*, 1980, **73**, 393–398.

52 C. Broyden, Notices of the American Mathematical Society, 1969, p. 670.

53 R. Fletcher, *Comput. J.*, 1970, **13**, 317–322.

54 D. Goldfarb, *Math. Comp.*, 1970, **24**, 23–26.

55 D. F. Shanno, *Math. Comp.*, 1970, **24**, 647–656.

56 J. V. Lauritsen, J. Kibsgaard, S. Helveg, H. Topsøe, B. S. Clausen, E. Lægsgaard and F. Besenbacher, *Nat. Nanotechnol.*, 2007, **2**, 53–58.

57 R. G. Dickinson and L. Pauling, *J. Am. Chem. Soc.*, 1923, **45**, 1466–1471.

58 S. Helveg, J. V. Lauritsen, E. Lægsgaard, I. Stensgaard, J. K. Nørskov, B. Clausen, H. Topsøe and F. Besenbacher, *Phys. Rev. Lett.*, 2000, **84**, 951.

59 G. Du, Z. Guo, S. Wang, R. Zeng, Z. Chen and H. Liu, *Chem. Commun.*, 2010, **46**, 1106–1108.

60 H. Schweiger, P. Raybaud, G. Kresse and H. Toulhoat, *J. Catal.*, 2002, **207**, 76–87.

61 N. Holmberg and K. Laasonen, *J. Phys. Chem. Lett.*, 2015, **6**, 3956–3960.

62 L. P. Hansen, Q. M. Ramasse, C. Kisielowski, M. Brorson, E. Johnson, H. Topsøe and S. Helveg, *Angew. Chem. Int. Ed.*, 2011, **50**, 10153–10156.

63 D. Le, T. B. Rawal and T. S. Rahman, *J. Phys. Chem. C*, 2014, **118**, 5346–5351.

64 M. G. Sensoy, D. Vinichenko, W. Chen, C. M. Friend and E. Kaxiras, *Phys. Rev. B*, 2017, **95**, 014106.

65 L.-P. Feng, J. Su, S. Chen and Z.-t. Liu, *Mater. Chem. Phys.*, 2014, **148**, 5–9.
66 H.-P. Komsa and A. V. Krasheninnikov, *Phys. Rev. B*, 2015, **91**, 125304.
67 N. Marković and P. N. Ross, *Surf. Sci. Rep.*, 2002, **45**, 117–229.
68 E. Skúlason, G. S. Karlberg, J. Rossmeisl, T. Bligaard, J. Greeley, H. Jónsson and J. K. Nørskov, *Phys. Chem. Chem. Phys.*, 2007, **9**, 3241–3250.
69 J. Lauritsen, M. Bollinger, E. Lægsgaard, K. W. Jacobsen, J. K. Nørskov, B. Clausen, H. Topsøe and F. Besenbacher, *J. Catal.*, 2004, **221**, 510–522.